

# Production of Charged $\pi^\pm$ , $K^\pm$ and $p/\bar{p}$ in Hadronic $Z^0$ Decays

The SLD Collaboration\*\*

Stanford Linear Accelerator Center  
Stanford University, Stanford, CA 94309

## ABSTRACT

We present improved measurements of identified charged hadron production over a wide momentum range at SLD, using the Cherenkov Ring Imaging Detector to identify clean samples of charged pions, kaons and protons. In addition to studying flavor-inclusive  $Z^0$  decays, we compare the production in light,  $c$  and  $b$  flavor events, and present a new comparison of light-quark and gluon jets, selected using the SLD vertex detector. Also, we update our comparison of hadron and antihadron production in light quark (rather than antiquark) jets, selected using the high SLC electron beam polarization. Differences between hadron and antihadron production at high momentum fraction provide precise measurements of leading particle production and new, stringent tests of fragmentation models.

*Contributed to: the International Europhysics Conference on High Energy Physics, 12–18 July, 2001, Budapest, Hungary, Ref: 670; and the XX<sup>th</sup> International Symposium on Lepton and Photon Interactions, 23–28 July, 2001, Rome, Italy.*

\*This work was supported by Department of Energy contract DE-AC03-76SF00515.

# 1 Introduction

The production of final state hadrons from primary hard partons, e.g. the quark and antiquark in  $e^+e^- \rightarrow Z^0 \rightarrow q\bar{q}$ , is currently believed to proceed in three stages. The first stage involves the radiation of gluons from the primary quark and antiquark, which in turn radiate gluons or split into  $q\bar{q}$  pairs until their virtuality approaches the hadron mass scale. Such a “parton shower” is calculable in perturbative QCD, for example in the Modified Leading Logarithm Approximation (MLLA) [1].

The second stage, in which these partons turn into “primary” hadrons, is not understood quantitatively, although several hadronization models exist. A simple model is the ansatz of Local Parton-Hadron Duality (LPHD) [1], which hypothesizes that distributions of kinematic quantities for a given hadron species are directly proportional to the parton distributions at some appropriate parton virtuality. This allows the prediction via MLLA QCD of the shapes of differential cross sections for primary hadrons, and of, for example, the energy- and mass-dependences of the peak of the distribution of  $\xi = -\ln(x_p)$ , where  $x_p = 2p/E_{cm}$ ,  $p$  is the hadron momentum and  $E_{cm}$  is the  $e^+e^-$  center-of-mass energy.

The third stage, in which unstable primary hadrons decay into final state hadrons, complicates the interpretation of inclusive measurements. It is desirable to remove the effects of these decays when comparing with the predictions of QCD+LPHD. Additional complications arise in jets initiated by heavy ( $c$  or  $b$ ) quarks in which the leading heavy hadrons carry a large fraction of the beam energy, restricting that available to other primary particles, and then decay into a number of secondary particles. It is thus also desirable to restrict measurements to events with light primary flavors.

A prediction of QCD is that a hard gluon will radiate more soft gluons at larger angles than a quark of equal energy, resulting in a wider jet with a higher multiplicity of softer gluons. This effect has been observed by several experiments in the multiplicity and inclusive distributions of charged tracks and energy clusters. However, no difference in the hadronization stage is expected, so that the relative production of different particle species should be the same in gluon jets as in light quark jets. There are currently few measurements in this area, with limited precision.

A particularly interesting aspect of jet fragmentation is the question of what happens to the primary quark or antiquark that initiated the jet. Many fragmentation models assume that the initial quark is “contained” as a valence constituent of a particular hadron, and that this “leading” hadron has on average a higher momentum than the other particles in the jet. This phenomenon has not been studied precisely for high-energy light-flavor jets, since it is difficult to identify the sign and flavor of the initial  $q/\bar{q}$  on a jet-by-jet basis. The quantification of leading particle effects could lead to ways to identify the primary flavor of arbitrary samples of jets, enabling a number of new measurements in  $e^+e^-$ , as well as in  $ep$  and  $p\bar{p}$ , collisions.

In this paper we present an analysis of  $\pi^\pm$ ,  $K^\pm$ , and  $p/\bar{p}$  production in hadronic  $Z^0$  decays collected by the SLC Large Detector (SLD), based upon the sample of 450,000

hadronic events obtained in runs of the SLAC Linear Collider (SLC) between 1996 and 1998. We update our measurements of differential cross sections in an inclusive sample of hadronic events of all flavors, and also in high-purity samples of light- ( $Z^0 \rightarrow u\bar{u}, d\bar{d}, s\bar{s}$ ),  $c$ - ( $Z^0 \rightarrow c\bar{c}$ ) and  $b$ -flavor ( $Z^0 \rightarrow b\bar{b}$ ) events. The unfolded differential cross sections for the light-flavor events are free from effects of heavy quark production and decay, and as such provide a more appropriate sample for comparison with QCD predictions, which generally assume massless quarks, although the influence of decay products of other unstable primary hadrons remains. We use these measurements to test the predictions of various fragmentation models.

In addition, we tag a high-purity sample of gluon jets in 3-jet events, and compare the production with light quark jets of the the same energy, in order to test the universality of the hadronization process. We also select samples of quark and antiquark jets from our light-flavor event sample, using the large forward-backward production asymmetry in polar angle inherent in collisions of highly polarized electrons with positrons. The differential cross sections are measured separately for hadrons and antihadrons in light-quark jets, and the observed differences are interpreted in terms of leading particle effects. These measurements provide precise, unique tests of fragmentation models.

## 2 The SLD and Hadronic Event Selection

A general description of the SLD can be found elsewhere [3]. The trigger and initial selection criteria for hadronic  $Z^0$  decays are described in Ref. [4]. This analysis used charged tracks measured in the Central Drift Chamber (CDC) [5] and Vertex Detector (VXD) [6], and identified using the Cherenkov Ring Imaging Detector (CRID) [7]. Momentum measurement is provided by a uniform axial magnetic field of 0.6T. The CDC and VXD give a momentum resolution of  $\sigma_{p_\perp}/p_\perp = 0.01 \oplus 0.0026p_\perp$ , where  $p_\perp$  is the track momentum transverse to the beam axis in GeV/ $c$ . In the plane normal to the beamline the centroid of the micron-sized SLC IP was reconstructed from tracks in sets of approximately thirty sequential hadronic  $Z^0$  decays to a precision of  $\sigma_{IP} \simeq 3 \mu\text{m}$ . Including the uncertainty on the IP position, the resolution on the charged track impact parameter ( $\delta$ ) projected in the plane perpendicular to the beamline is  $\sigma_\delta = 8 \oplus 29/(p \sin^{3/2} \theta) \mu\text{m}$  where  $\theta$  is the track polar angle with respect to the beamline. The CRID comprises two radiator systems that allow the identification of charged pions with high efficiency and purity in the momentum range 0.3–35 GeV/ $c$ , charged kaons in the ranges 0.75–6 GeV/ $c$  and 9–35 GeV/ $c$ , and protons in the ranges 0.75–6 GeV/ $c$  and 10–46 GeV/ $c$  [8]. The event thrust axis [9] was calculated using energy clusters measured in the Liquid Argon Calorimeter [10].

A set of cuts was applied to the data to select well-measured tracks and events well contained within the detector acceptance. Charged tracks were required to have a distance of closest approach transverse to the beam axis within 5 cm, and within 10 cm along the axis from the measured IP, as well as  $|\cos \theta| < 0.80$ , and  $p_\perp > 0.15$

	Efficiency for $Z^0 \rightarrow$			Purity of $Z^0 \rightarrow$		
	$u\bar{u}, d\bar{d}, s\bar{s}$	$c\bar{c}$	$b\bar{b}$	$u\bar{u}, d\bar{d}, s\bar{s}$	$c\bar{c}$	$b\bar{b}$
light-tag	0.734	0.190	0.010	0.928	0.064	0.008
$c$ -tag	0.049	0.551	0.105	0.203	0.641	0.156
$b$ -tag	0.001	0.024	0.815	0.005	0.023	0.972

Table 1: Tagging efficiencies for simulated events in the three flavor categories to be tagged as light,  $c$  or  $b$ . The three rightmost columns indicate the composition of each simulated tagged sample assuming SM relative flavor production.

GeV/c. Events were required to have a minimum of five such tracks, a thrust axis polar angle w.r.t. the beamline,  $\theta_T$ , within  $|\cos \theta_T| < 0.71$ , and a charged visible energy  $E_{vis}$  of at least 20 GeV, which was calculated from the selected tracks assigned the charged pion mass. The efficiency for selecting a well-contained  $Z^0 \rightarrow q\bar{q}(g)$  event was estimated to be above 96% independent of quark flavor. The VXD, CDC and CRID were required to be operational, resulting in a selected sample of roughly 308,000 events, with an estimated non-hadronic background contribution of  $0.10 \pm 0.05\%$  dominated by  $Z^0 \rightarrow \tau^+\tau^-$  events.

Samples of events enriched in light and  $b$  primary flavors were selected using tracks with well measured impact parameters  $\delta$  with respect to the IP. For each event we define  $n_{sig}^{evt}$  as the number of tracks with impact parameter greater than three times its estimated error,  $\delta > 3\sigma_\delta$ . We also run a topological vertex finding algorithm [11] on the set of tracks in each hemisphere and consider the  $p_t$ -corrected mass  $M_{pt}$  of any vertex found. Any event containing a vertex with  $M_{pt} > 2 \text{ GeV}/c^2$  was assigned to the  $b$ -tagged sample; an event without such a vertex, but having either  $n_{sig} > 2$  or a vertex with  $M_{pt} > 0.5 \text{ GeV}/c^2$ ,  $p_{vtx} > 2 \text{ GeV}/c$  and  $p_{vtx} - 14M_{pt} > -10$  was assigned to the  $c$ -tagged sample; events with no found vertices and  $n_{sig} = 0$  were assigned to the light flavor sample. The light,  $c$  and  $b$  samples comprised 101,000, 34,000 and 40,000 events, respectively; selection efficiencies and sample purities were estimated from our Monte Carlo simulation and are listed in table 1.

A sample of gluon jets was selected from 3-jet events, defined by applying the Durham jetfinding algorithm to the set of charged tracks in the event with a resolution parameter of  $y_{cut} = 0.005$ . The jets energies were rescaled using massless kinematics and the two lower energy jets were considered a gluon candidates if the angle between their axes exceeded 20 degrees. The topological vertex finder was run on the set of vertex quality tracks in each jet and the  $n_{sig}^{jet}$  was calculated for each jet. If a vertex with  $M_{pt} > 0.75 \text{ GeV}/c^2$  and  $p_{vtx} > 3 \text{ GeV}/c$  was found in one of the two lower energy jets, then the other was tagged as a gluon jet if it contained no vertex, had an energy greater than 3 GeV and the polar angle of its axis satisfied  $|\cos \theta_{jet}| < 0.7$ . This results in 13,510 jets tagged with an estimated 92% gluon purity. The distribution of

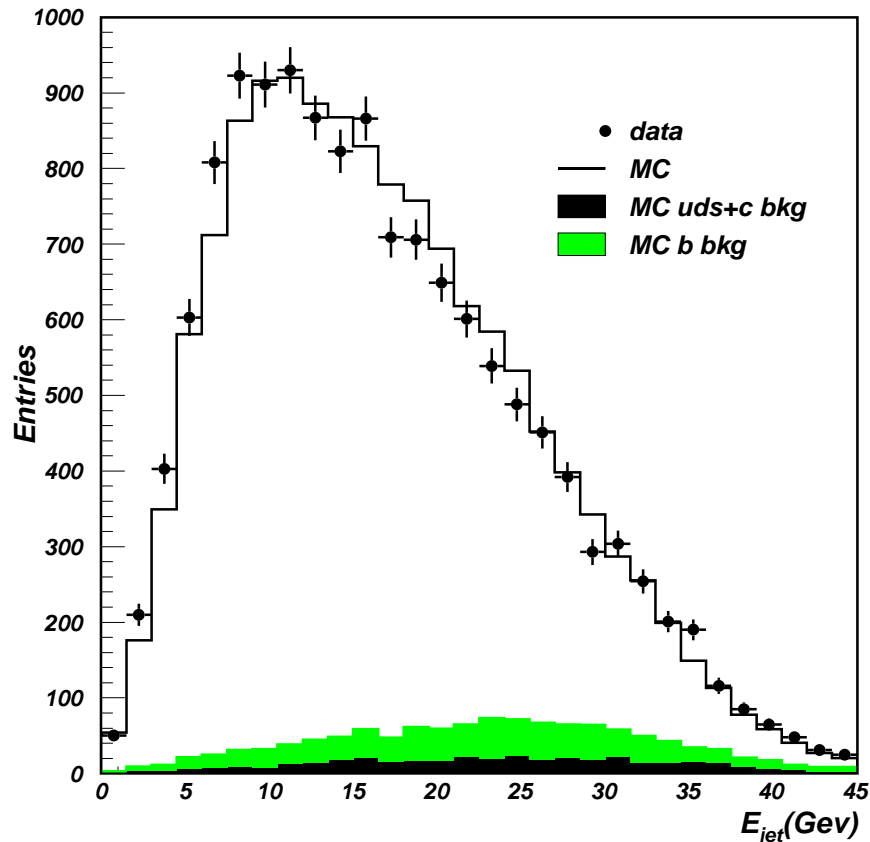


Figure 1: Distribution of the reconstructed energies of the tagged gluon jets in the data (dots) and simulation (histogram). The simulated contributions from non gluon jets are indicated.

tagged gluon jet energy is shown in fig. 1; the simulation is consistent with the data and the background contributions are indicated, the dominant source being  $b/\bar{b}$  jets. We compare with a light-mixture sample, comprising any of the two lowest energy jets in 3-jet events tagged as light-flavor, as described above, with an axis satisfying  $|\cos \theta_{jet}| < 0.7$ . This sample is estimated to be 46% true gluon jets and 48% light quark jets, with a small background from  $c$  and  $b$  jets. As a cross-check we also consider a  $b$ -mixture and a  $c$ -mixture, defined as the two lowest energy jets in events in which the highest energy jet contained a  $b$  or  $c$  vertex (see above), respectively.

Separate samples of hemispheres enriched in light-quark and light-antiquark jets were selected from the light-tagged event sample by exploiting the large electroweak forward-backward production asymmetry wrt the beam direction. The event thrust axis was used to approximate the initial  $q\bar{q}$  axis and was signed such that its  $z$ -component was positive,  $\hat{t}_z > 0$ . Events in the central region of the detector, where the production asymmetry is small, were removed by the requirement  $|\hat{t}_z| > 0.2$ , leaving 125,000 events. The quark-tagged hemisphere in events with left-(right-)handed electron beam was defined to comprise the set of tracks with positive (negative) mo-

momentum projection along the signed thrust axis. The remaining tracks in each event were defined to be in the antiquark-tagged hemisphere. The sign and magnitude of the electron beam polarization were measured for every event. For the selected event sample, the average magnitude of the polarization was 0.73. Using this value and assuming Standard Model couplings at tree-level, the purity of the quark-tagged sample is 0.73.

For the purpose of estimating the efficiency and purity of the event flavor tagging and the particle identification, we made use of a detailed Monte Carlo (MC) simulation of the detector. The JETSET 7.4 [12] event generator was used, with parameter values tuned to hadronic  $e^+e^-$  annihilation data [13], combined with a simulation of  $B$ -hadron decays tuned [14] to  $\Upsilon(4S)$  data and a simulation of the SLD based on GEANT 3.21 [15]. Inclusive distributions of single-particle and event-topology observables in hadronic events were found to be well described by the simulation [4].

### 3 Measurement of the Charged Hadron Fractions

Charged tracks were identified as pions, kaons or protons, in the CRID using a likelihood technique [16]. Information from the liquid (gas) radiator only was used for tracks with  $p < 2.5$  ( $p > 7.5$ ) GeV/c; in the overlap region,  $2.5 < p < 7.5$  GeV/c, liquid and gas information was combined. Additional track selection cuts were applied to remove tracks that scattered through large angles before exiting the CRID and to ensure that the CRID performance was well-modelled by the simulation. Tracks were required to have at least 40 CDC hits, at least one of which was in the outermost superlayer, to extrapolate through an active region of the appropriate radiator(s), and to have at least 80% of their expected liquid and/or gas ring contained within a sensitive region of the CRID TPCs. The latter requirement included rejection of tracks with  $p > 2.5$  GeV/c for which there was a saturated CRID hit (from passage of minimum-ionizing particles) within a 2.5 cm radius (the maximum ring radius) of the expected gas ring center; for momenta in the range  $7.5 < p < 20$  GeV/c, this cut was tightened to 5 cm, assuring containment of 100 Tracks with  $p < 7.5$  GeV/c were required to have a saturated hit within 1 cm of the extrapolated track if it went through an active TPC, and tracks with  $p > 2.5$  GeV/c were required to have either such a saturated hit or the presence of at least four hits consistent with a liquid ring. These cuts accepted 82, 80, 49 and 75% of tracks within the barrel acceptance in the momentum ranges  $p < 2.5$ ,  $2.5 < p < 7.5$ ,  $7.5 < p < 20$ , and  $p > 20$  GeV/c, respectively. For momenta below 2 GeV/c, only negatively charged tracks were used to reduce the background from protons produced in interactions with the detector material.

For tracks with  $p < 2.5$  ( $p > 2.5$ ) GeV/c, we define a particle to be identified as type  $j$ , where  $j = \pi, K, p$ , if  $\mathcal{L}_j$  exceeds both of the other log-likelihoods by at least 5 (3) units. Efficiencies for identifying selected particles of true type  $i$  as type  $j$  were determined where possible from the data, using tracks from tagged  $K_s^0$ ,  $\tau^\pm$  and  $\Lambda^0$  de-

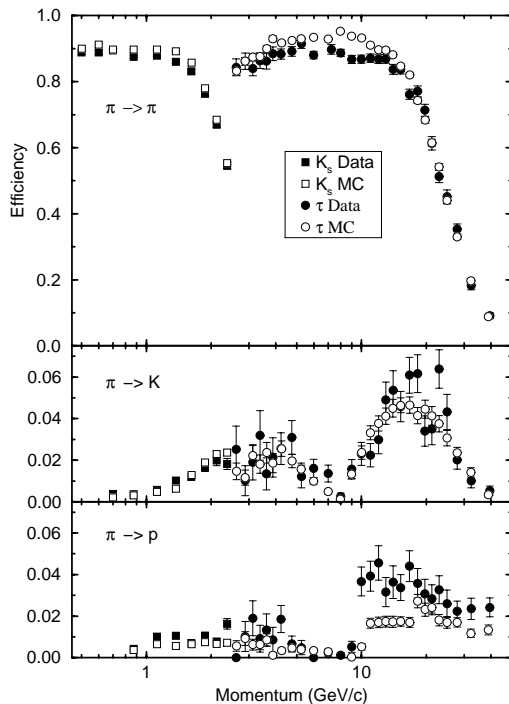


Figure 2: Calibration of the pion identification efficiencies using tracks from tagged  $K_s^0$  and  $\tau^\pm$  decays.

cays, as described in [8]. An example is shown in fig. 2. A detailed Monte Carlo (MC) simulation of the detector was then used to make small corrections to these measurements, and to derive the remaining efficiencies from those measured. These efficiencies are parametrized in terms of continuous functions in each of the three momentum ranges, and are shown in fig. 3, in which the pairs of lines represent our estimated efficiencies plus and minus their systematic uncertainties. For the diagonal entries, these uncertainties correspond to statistical errors on the parameters fitted from the data, and are completely positively correlated across each of the three momentum regions. For the off-diagonal terms, representing misidentification rates, a more conservative 25% relative error was assigned at all points to account for the limited experimental constraints on the momentum dependence. These errors are also strongly positively correlated among momenta. The diagonal elements peak near or above 0.9 and the pion coverage is continuous from 0.5 GeV/c up to approximately 35 GeV/c. There is a gap in the kaon-proton separation between 7 and 10 GeV/c due to limited resolution of the liquid system and the fact that both particles are below Cherenkov threshold in the gas system. The proton coverage extends to the beam momentum. Misidentification rates are typically less than 0.03, with peak values of up to 0.07.

In each momentum bin we measured the fractions of the selected tracks that were identified as  $\pi$ ,  $K$  and  $p$ . The observed fractions were related to the true production fractions by an efficiency matrix, composed of the values in fig. 3 for that bin. This matrix was inverted and used to unfold our observed identified particle rates. This

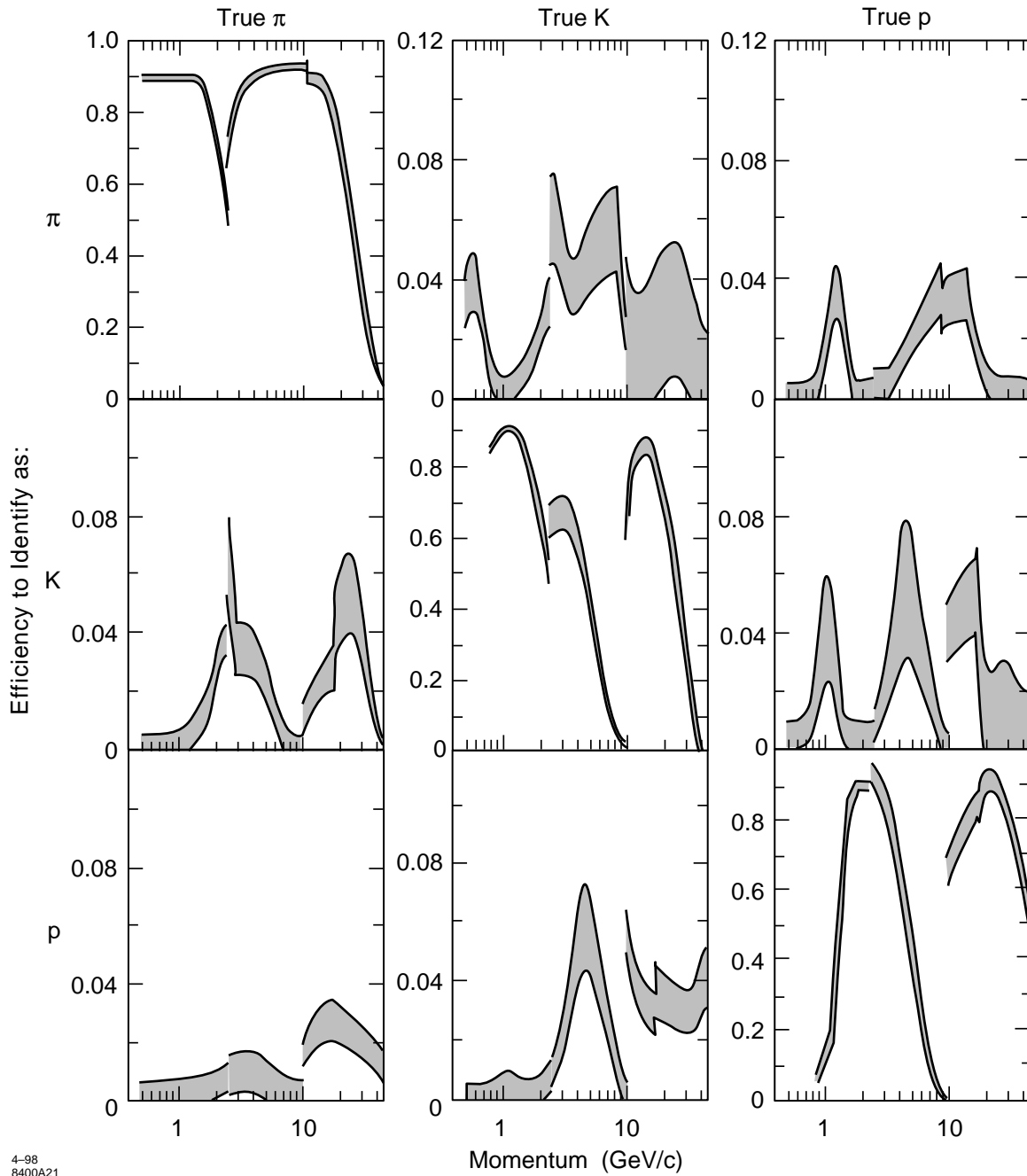


Figure 3: Calibrated identification efficiencies for tracks used in the charged hadron fractions analysis. The separations between the pairs of lines represent the systematic uncertainties, which are strongly correlated between momenta.



analysis procedure does not require that the sum of the charged particle fractions be unity; instead the sum was used as a consistency check and was found to be within statistical errors of unity for all momenta. In some momentum regions we cannot distinguish two of the three species, so the procedure was reduced to a  $2 \times 2$  matrix analysis and we present only the fraction of the identified species, i.e. protons above 35 GeV/c and pions between 6 and 9.5 GeV/c.

Electrons and muons were not distinguished from pions in this analysis; this background was estimated from the simulation to be about 5% in the inclusive flavor sample, predominantly from  $c$ - and  $b$ -flavor events. The flavor-inclusive fractions were corrected using the simulation for the lepton backgrounds, as well as for the effects of beam-related backgrounds, particles interacting in the detector material, and particles with large flight distance, such that the conventional definition of a final-state charged hadron is recovered, namely charged pions, kaons or protons that are either from the primary interaction or decay products of particles with lifetime less than  $3 \times 10^{-10}$ s.

The measured charged particle fractions for inclusive hadronic  $Z^0$  decays are shown in fig. 4. The errors on the points below 15 GeV/c are dominated by the systematic uncertainties on the identification efficiencies and are strongly positively correlated across the entire momentum range. For  $p > 15$  GeV/c the errors have roughly equal statistical and systematic contributions, and the systematic errors are positively correlated and increase in magnitude with momentum.

Pions are seen to dominate the charged hadron production at low momentum, and to decline steadily in fraction as momentum increases. The kaon fraction rises steadily to about one-third at high momentum. The proton fraction rises to a maximum of about one-tenth at about 10 GeV/c, then declines slowly. At high  $x_p$ , the pion and kaon fractions appear to be converging. This convergence could indicate reduced strangeness suppression at high momentum, or that production is becoming dominated by leading particles, such that kaons from  $s\bar{s}$  events are as common as pions from  $u\bar{u}$  and  $d\bar{d}$  events. Where the momentum coverage overlaps, these measured fractions were found to be in agreement with our previous results [8] and with other measurements at the  $Z^0$  [17, 18, 19]. Measurements based on ring imaging [8, 17] and those based on ionization energy loss rates [18, 19] cover complementary momentum ranges and can be combined to provide continuous coverage over the range  $0.2 < p < 35$  GeV/c.

In fig. 5 we compare our measured charged hadron fractions with the predictions of the JETSET 7.4 [12], UCLA [20] and HERWIG 5.8 [21] fragmentation models, using default parameters. The momentum dependence of each fraction is reproduced qualitatively by all three models. The HERWIG and UCLA predictions for the pion fraction are high at intermediate  $x_p$ ; the three model predictions differ widely at very high  $x_p$ , but the statistics of the data are not sufficient to distinguish between them. All three predictions for the kaon fraction are too low (high) at small (large)  $x_p$ . The JETSET prediction for the proton fraction is too high at all  $x_p$ ; those of HERWIG and UCLA show structure in the proton fraction at large  $x_p$  that is inconsistent with the data.

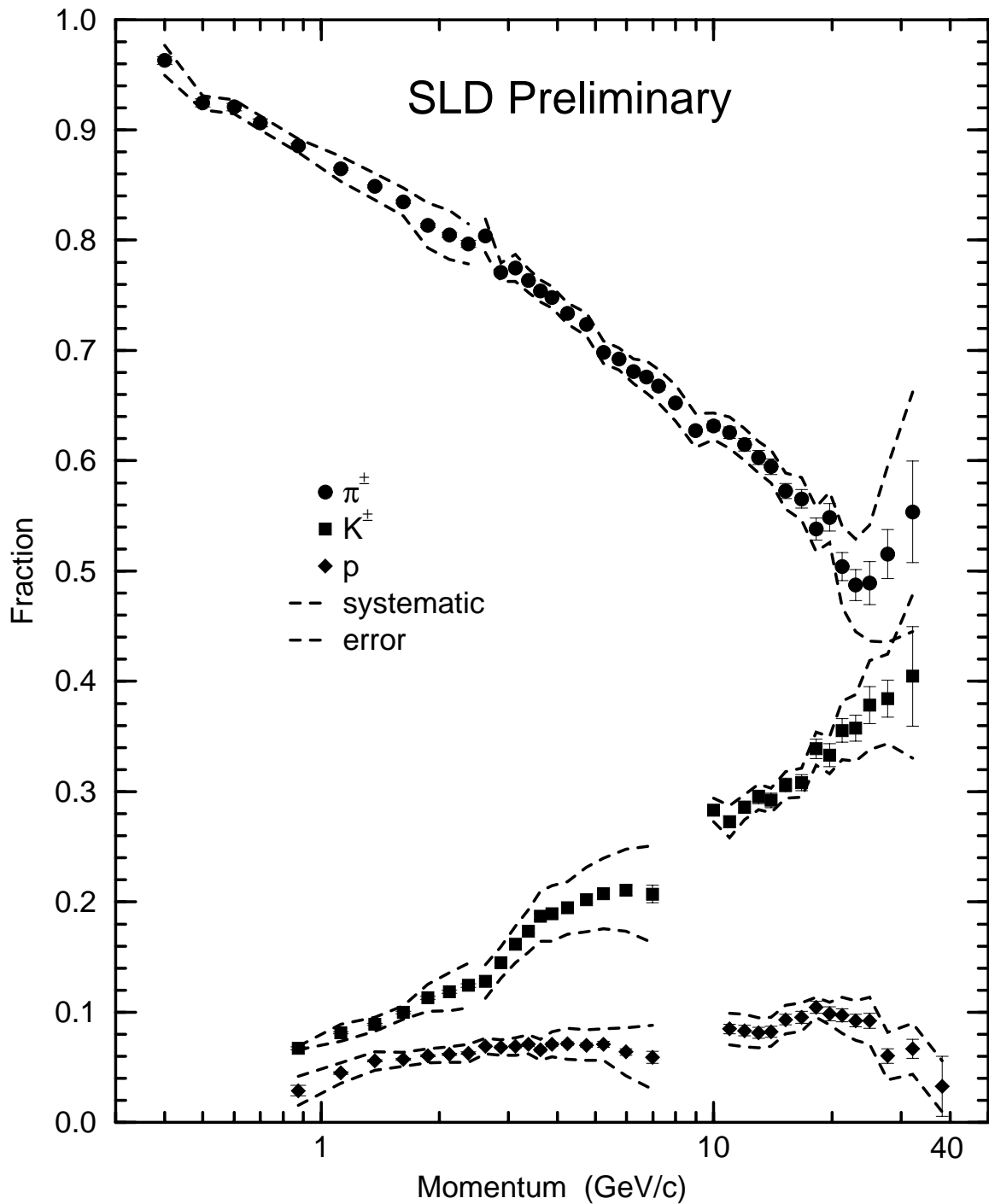


Figure 4: Measured charged hadron production fractions in hadronic  $Z^0$  decays. The circles represent the  $\pi^\pm$  fraction, the squares the  $K^\pm$  fraction, the diamonds the  $p/\bar{p}$  fraction. The error bars are statistical only. The dotted lines indicate the systematic errors, which are strongly correlated between momenta (see text)

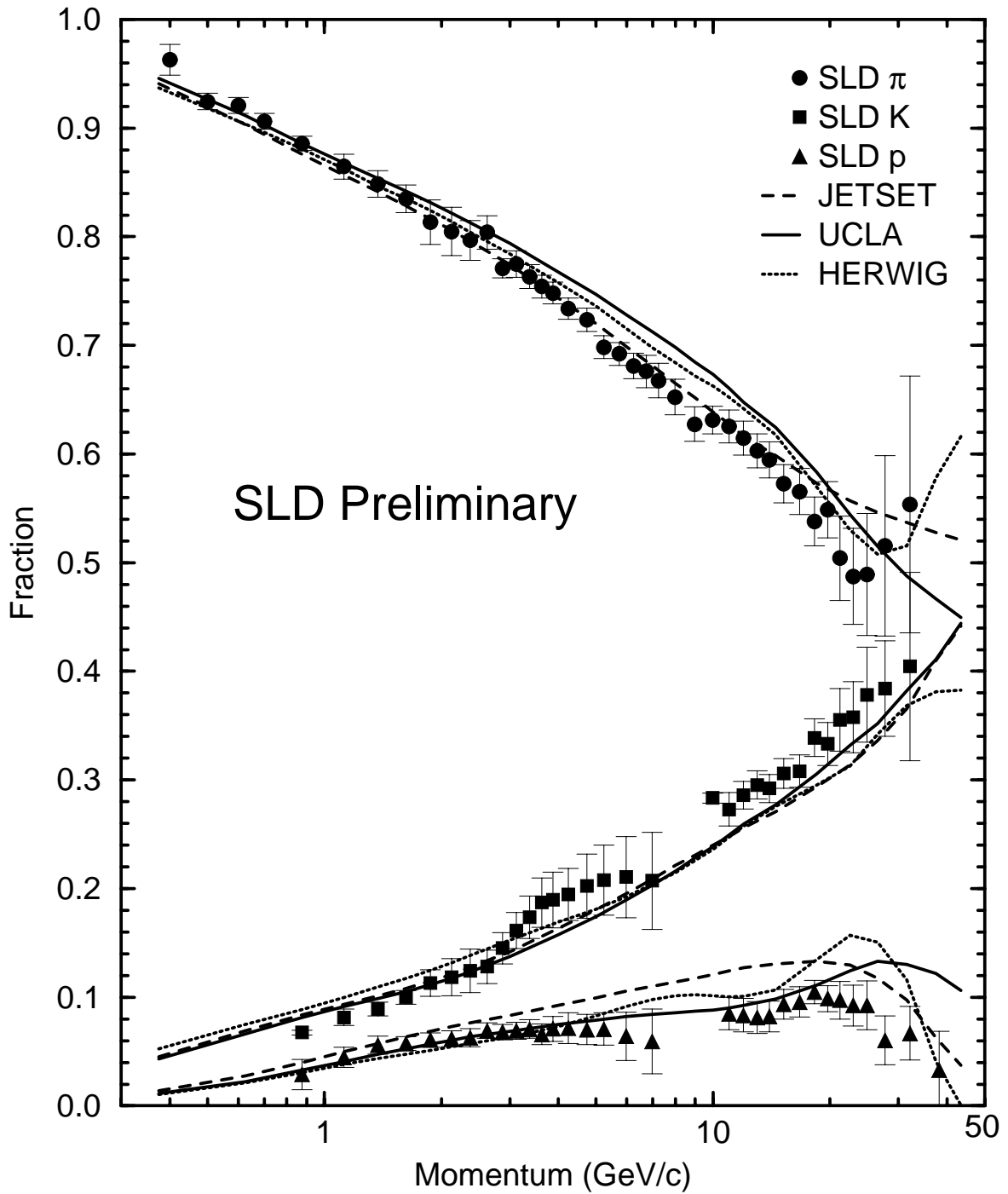


Figure 5: Comparison of the charged hadron fractions in flavor-inclusive events with the predictions of three fragmentation models.

## 4 Flavor-Dependent Analysis

The analysis was repeated separately on the high-purity light-,  $c$  and  $b$ -tagged event samples described in section 2. In each momentum bin the measured differential cross sections  $r_j^{meas}$  of each hadron species for these three samples,  $j = \text{light-tag, } c\text{-tag, } b\text{-tag}$ , were unfolded by inverting the relations:

$$r_j^{meas} = \frac{\sum_i b_{ij} \epsilon_{ij} R_i r_i^{true}}{\sum_i \epsilon_{ij} R_i} \quad (1)$$

to yield true differential cross sections  $r_i^{true}$  in events of the three flavor types,  $i = 1, 2, 3$ , corresponding to  $Z^0 \rightarrow u\bar{u}, d\bar{d}, s\bar{s}$ ,  $Z^0 \rightarrow c\bar{c}$  and  $Z^0 \rightarrow b\bar{b}$ . Here,  $R_i$  is the fraction of hadronic  $Z^0$  decays of flavor type  $i$ , taken from [23],  $\epsilon_{ij}$  is the event tagging efficiency matrix, estimated from the simulation and listed in table 1, and  $b_{ij}$  represents the momentum-dependent bias of tag  $j$  toward selecting events of flavor  $i$  that contain hadrons of the type in question. The diagonal bias values [22] are within a few percent of unity, reflecting a small multiplicity dependence of the flavor tags. The off-diagonal bias values are larger, but these have little effect on the unfolded results.

In fig. 6 we compare our measured charged hadron fractions in light-flavor flavor events with the predictions of the three fragmentation models. Qualitatively there is little difference between these data and those for the inclusive sample (fig. 4), however these are more relevant for comparison with QCD predictions based on the assumption of massless primary quark production, as well as for determining parameters in fragmentation models. We observe the same general differences between the predictions of the three fragmentation models and the data as were seen above in the flavor-inclusive sample. This indicates that these deficiencies are in the fragmentation simulation and not simply in the modelling of heavy hadron production and decay.

In fig. 7 we show the ratios of production in  $b$ - to light-flavor and  $c$ - to light-flavor events for the three species. The systematic errors on the particle identification largely cancel in these ratios, and the resulting errors are predominantly statistical. There is greater production of charged pions in  $b$ -flavor events at low momentum, with an approximately constant ratio for  $0.02 < x_p < 0.07$ . The production charged kaons is approximately equal in the two samples at  $x_p = 0.02$ , but the relative production in  $b$ -flavor events then increases with  $x_p$ , peaking at  $x_p \approx 0.07$ . There is approximately equal production of protons in  $b$ -flavor and light-flavor events below  $x_p = 0.15$ . For  $x_p > 0.1$ , production of all these particle species falls faster with increasing momentum in  $b$ -flavor events. These features are consistent with expectations based on the known properties of  $Z^0 \rightarrow b\bar{b}$  events, namely that a large fraction of the event energy is carried by the leading  $B$ - and  $\bar{B}$ -hadrons, which decay into a large number of lighter particles. Also shown in fig. 7 are the predictions of the three fragmentation models, which reproduce these features qualitatively, although HERWIG overestimates the pion and kaon ratios by a large factor at low  $x_p$ .

There is higher kaon production in  $c$ -flavor events than in light-flavor events at  $x_p \sim 0.1$ , reflecting the tendency of  $c$ -jets to produce a fairly hard charmed hadron

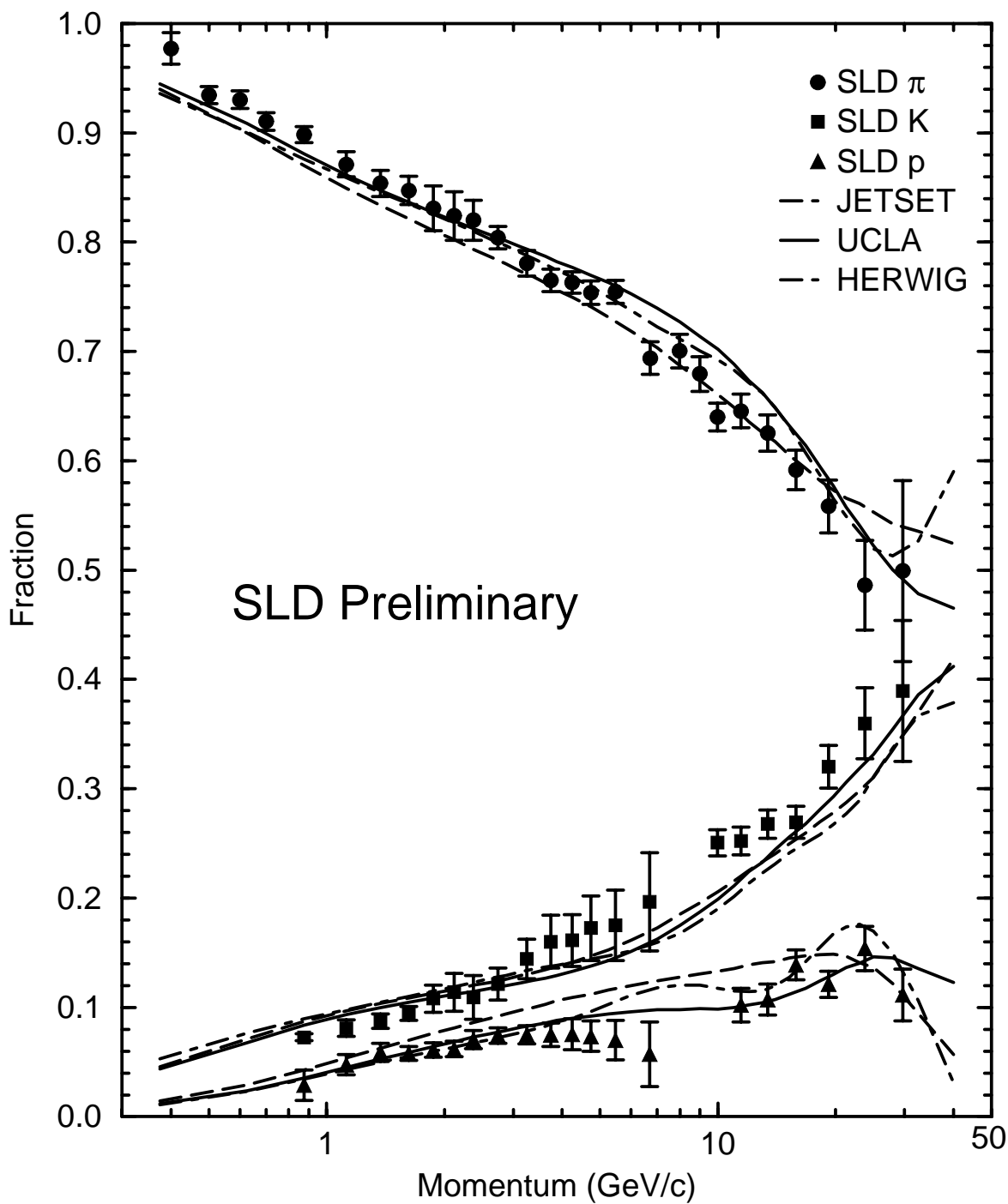


Figure 6: Comparison of our charged hadron fractions in light-flavor events with the predictions of three fragmentation models.

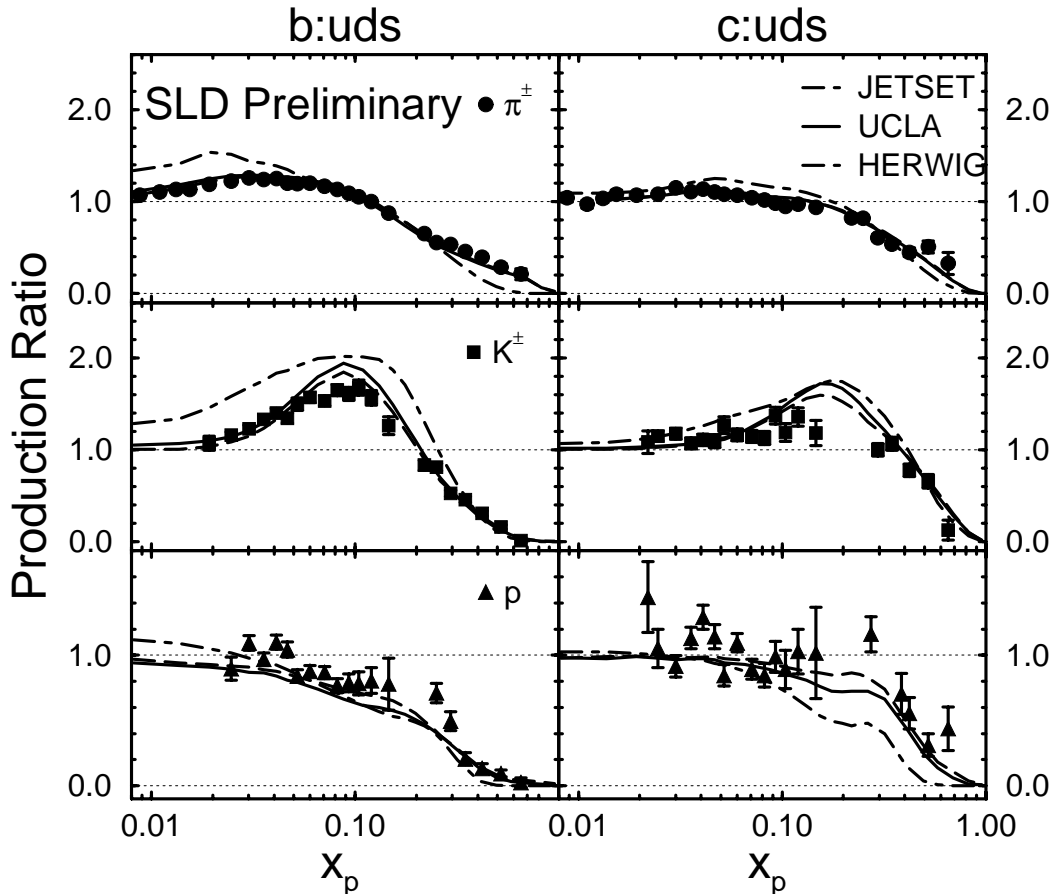


Figure 7: Ratios of production rates in  $b$ -flavor events to those in light-flavor events, along with the predictions of three fragmentation models.

whose decay products include a kaon carrying a large fraction of its momentum. There are fewer additional charged pions produced in  $D$  decays than in  $B$  decays, so that pion production is only slightly higher in  $c$ -flavor events at very small  $x_p$ . The pion  $c$ :light ratio starts to cut off at a larger value,  $x_p \approx 0.3$ , than the corresponding  $b$ :light ratio, attributable to the lower average decay multiplicity and softer fragmentation function of  $D$  hadrons, and the kaon and proton ratios are consistent with this cutoff point. Again, all three fragmentation models reproduce the data qualitatively, although HERWIG overestimates the pion ratio at small  $x_p$ , as it did in the  $b$ :light case, and underestimates the proton ratio at large  $x_p$ .

## 5 Relative Production in Gluon Jets

The fractions analysis was then repeated on the high-purity gluon jet sample described in section 2, as well as on the light-,  $c$ - and  $b$ -mixture samples. The results for the latter two samples were found to be consistent with the predictions of the simulation, indicating that the small  $c$  and  $b$  jet backgrounds in both the gluon-tagged and light-mixture samples are well modelled.

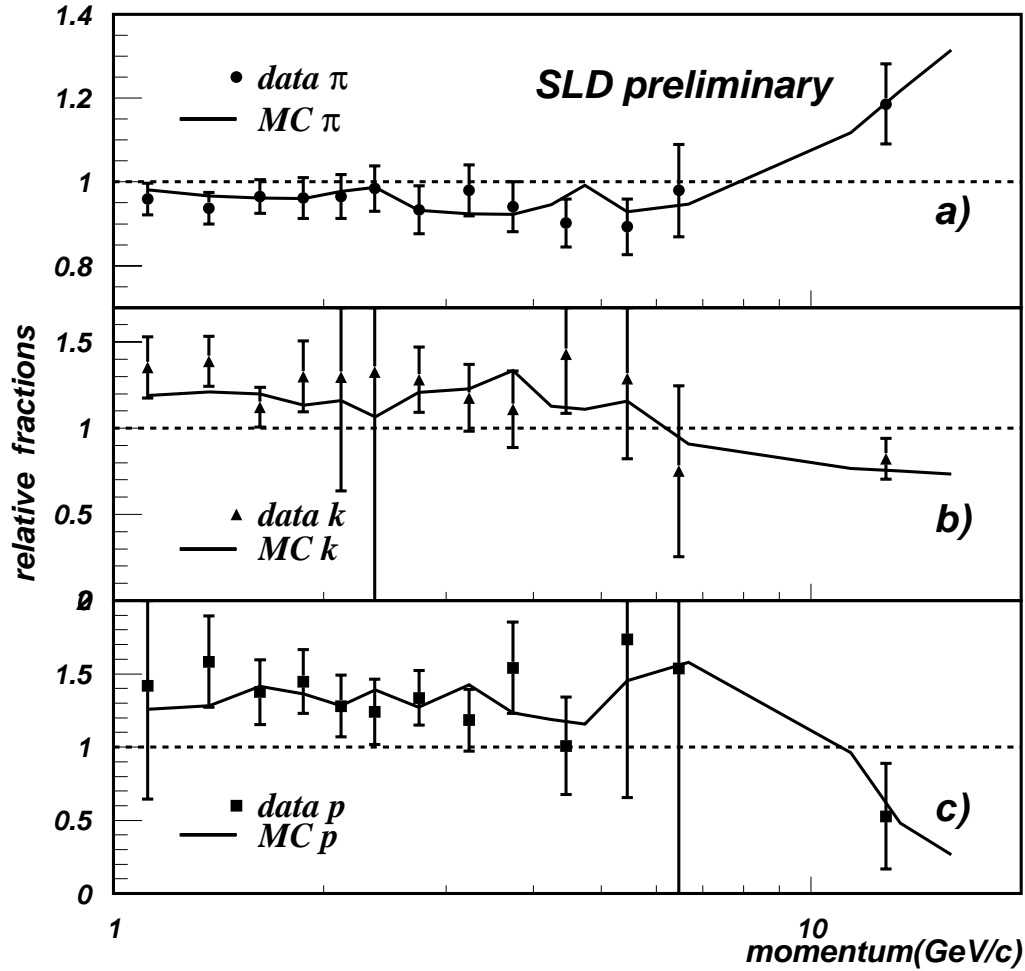


Figure 8: Ratios of fractions in  $g$ -tagged jets to those in light-mixture jets, along with the predictions of our simulation.

As a first comparison, we show in fig. 8 the ratio of the pion fraction measured in the gluon-tagged sample to that measured in the light-mixture sample, along with the corresponding ratios for kaons and protons. There are significant deviations from unity in these ratios, however they are reproduced by our simulation, so can be explained as kinematic biases due, for example, to the different average jet energy in the gluon-tagged and light-mixture samples. We thus conclude that at the level of our errors of a few percent, the relative production properties of charged pions, kaons and protons are the same.

## 6 Leading Particle Effects

We extended [24] these studies to look for differences between particle and antiparticle production in quark (rather than antiquark) jets, in order to address the question of whether e.g. a primary  $u$ -initiated jet contains more particles that contain a valence  $u$ -quark (e.g.  $\pi^+$ ,  $K^+$ ,  $p$ ) than particles that do not (e.g.  $\pi^-$ ,  $K^-$ ,  $\bar{p}$ ). To this end we

used the light quark- and antiquark-tagged hemispheres described in section 2.

We measured the production rates per light quark jet

$$R_h^q = \frac{1}{2N_{evts}} \frac{d}{dx_p} \left[ N(q \rightarrow h) + N(\bar{q} \rightarrow \bar{h}) \right], \quad (2)$$

$$R_{\bar{h}}^q = \frac{1}{2N_{evts}} \frac{d}{dx_p} \left[ N(q \rightarrow \bar{h}) + N(\bar{q} \rightarrow h) \right], \quad (3)$$

where:  $q$  and  $\bar{q}$  represent light-flavor quark and antiquark jets respectively;  $N_{evts}$  is the total number of events in the sample;  $h$  represents any of the identified hadrons  $\pi^-$ ,  $K^-$ , and  $p$ , and  $\bar{h}$  indicates the corresponding antiparticle. Then, for example,  $N(q \rightarrow h)$  is the number of hadrons of type  $h$  in light quark jets.

The charged hadron fractions analysis was repeated separately on the positively and negatively charged tracks in each of the quark- and antiquark-tagged samples. Results for the positively charged tracks in the quark-tagged sample and the negatively-charged tracks in the antiquark-tagged sample were consistent, so these two samples were combined and labelled as positively charged hadrons from light quark jets, yielding measured values of  $R_{\pi^+}^q$ ,  $R_{K^+}^q$ , and  $R_p^q$  in the tagged samples. The same procedure applied to the remaining tracks yielded  $R_{\pi^-}^q$ ,  $R_{K^-}^q$ , and  $R_{\bar{p}}^q$ .

It is essential to understand the contributions to these rates from heavy-flavor events, which are typically large in the momentum range we cover and show substantial differences between hadron and antihadron due to decay products of the heavy hadrons. This motivated our use of light-tagged events, and the residual heavy flavor contributions were estimated from the simulation to be typically 15% of the observed hadrons. This estimate was applied as a correction, yielding differential cross sections per light-quark-tagged jet. The effect of this correction on the results was negligible compared with the statistical errors.

For each hadron type, differential cross sections in light quark jets were then extracted by correcting for the light-tag bias and unfolding for the effective quark (vs. antiquark) purity. The purity was estimated from the simulation to be 0.72, which is slightly lower than the value of 0.73 noted in section 2, reflecting the cutoff in acceptance of the barrel CRID at  $|\cos \theta| = 0.68$ .

The measured differential cross sections per light quark jet are shown in fig 9. The errors shown are the sum in quadrature of statistical errors and those systematic errors arising from uncertainties in the heavy-flavor background correction and the effective quark purity; the statistical errors dominate this total. Systematic errors common to hadron and antihadron, such as those due to their identification efficiencies, are not included,

In all cases the hadron and antihadron differential cross sections are consistent at low  $x_p$ . For charged pions there are small differences at high  $x_p$ , and for the other particles there are substantial differences, all of which appear to increase with increasing  $x_p$ . It is convenient to show these data in the form of the difference between hadron



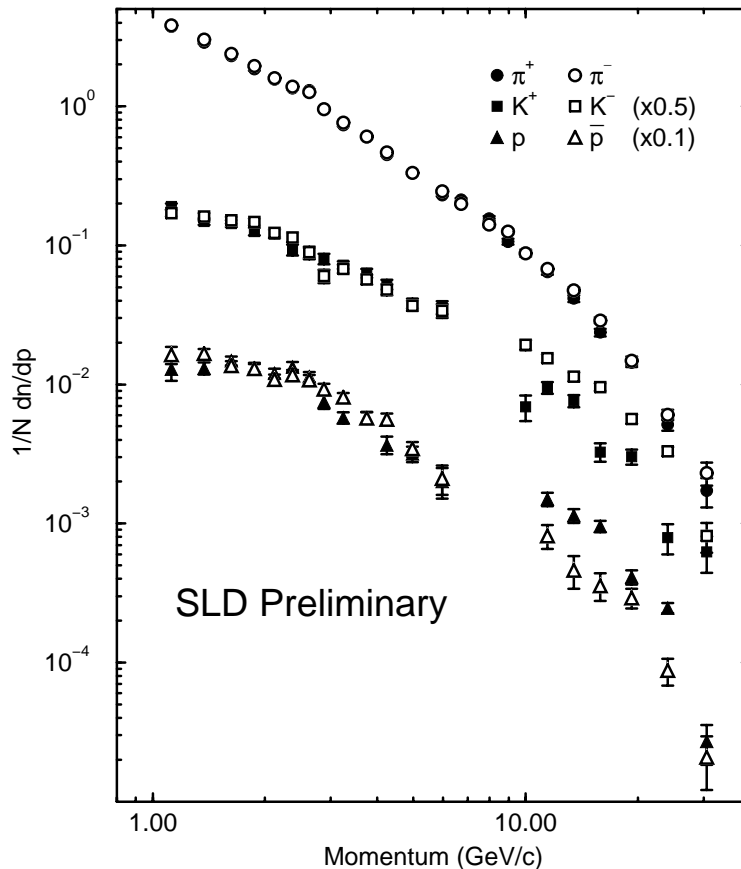


Figure 9: Scaled momentum distributions of identified particles and their antiparticles per light quark ( $u$ ,  $d$ ,  $s$ ) jet.

and antihadron differential cross sections normalized by the sum:

$$D_h = \frac{R_h^q - R_{\bar{h}}^q}{R_h^q + R_{\bar{h}}^q}, \quad (4)$$

The common systematic errors cancel explicitly in this variable. Results are shown in fig 10, along with our previous [8] similar results for the strange vector meson  $K^{*0}$  and the  $\Lambda^0$  hyperon. A value of zero corresponds to equal production of hadron and antihadron, and the data are consistent with zero at low  $x_p$ . A value of +1 (-1) corresponds to complete dominance of (anti)hadrons  $h$ .

The baryon results are most straightforward to interpret. Since baryons contain valence quarks and not antiquarks, the excess of baryons over antibaryons in light quarks jets provides clear evidence for the production of leading baryons at high scaled momentum. The data suggest that the effect increases with  $x_p$ .

The interpretation for the mesons is more complicated, since they contain one valence quark along with one antiquark. All down-type quarks are produced equally and with the same SM forward-backward asymmetry in  $Z^0$  decays, so that if a leading neutral particle such as  $K^{*0}$  ( $d\bar{s}$ ) were produced equally in  $d$  and  $\bar{s}$  jets then one would observe  $D_{\bar{K}^{*0}} = 0$ . In the case of charged mesons such as  $\pi^-$  ( $d\bar{u}$ ), the different production rates and forward-backward asymmetries of up- and down-type quarks

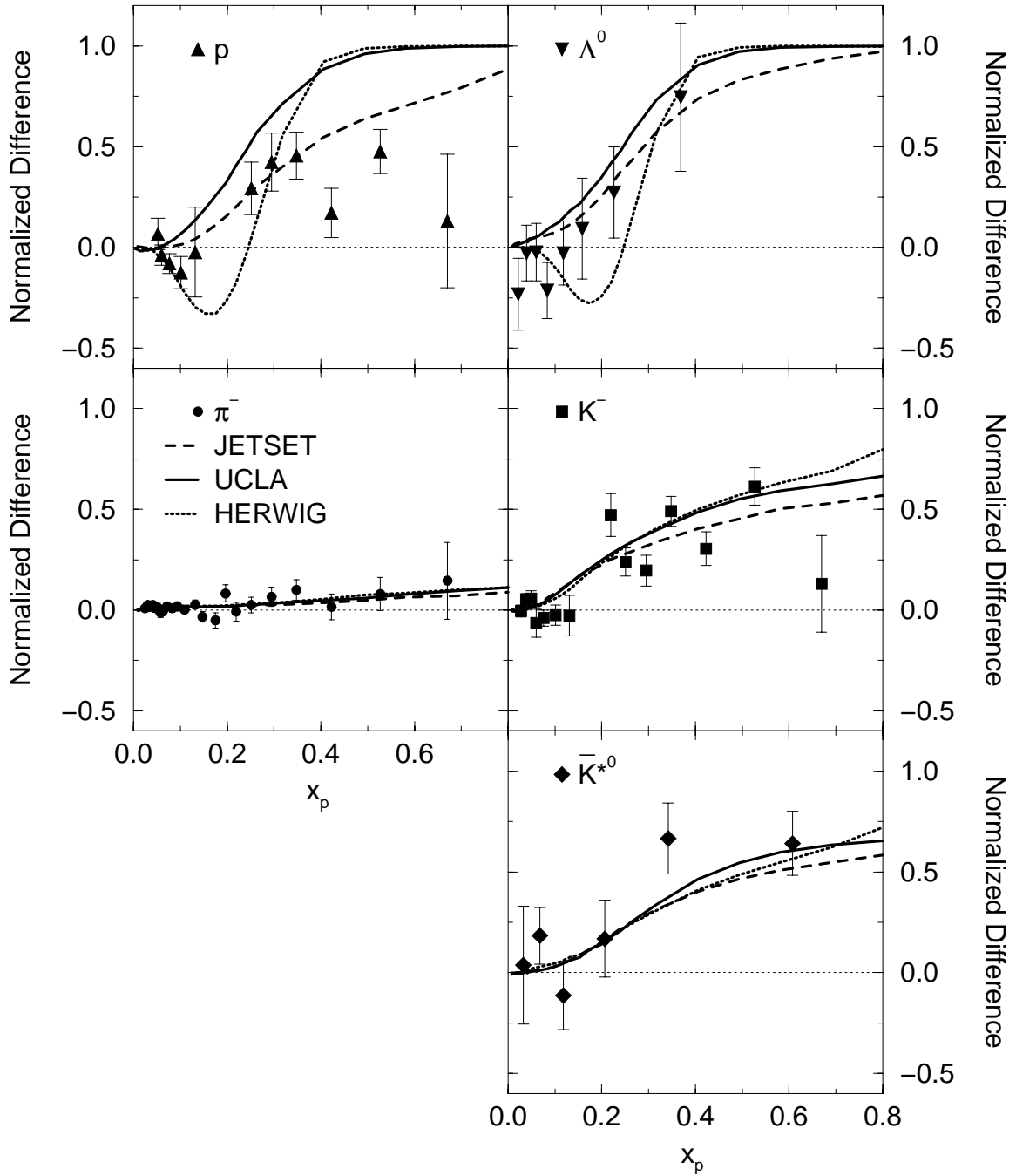


Figure 10: Normalized production differences between hadrons and their respective antihadrons in light quark jets. Also shown are the predictions of three fragmentation models.

cause a nonzero dilution of leading particle effects. At the  $Z^0$ , equal leading pion production in  $u$ - and  $d$ -jets would lead to a dilution factor of 0.27.

Our measured  $D_{\pi^-}$  are consistently above zero at high  $x_p$ , and consistently below  $0.27D_p$ , although statistically consistent at each point with both. This suggests that leading primary pions are produced, but indicates that nonleading production of pions must be relatively large. This could be due to a very soft leading pion momentum distribution and/or a large “background” contribution from decays of  $\rho^0$ ,  $K^*$ , etc. Our measured  $D_{K^-}$  are well above both zero and  $0.27D_p$  for  $x_p > 0.2$ . This indicates both substantial production of leading  $K^\pm$  mesons at high momentum, and a depletion of leading kaon production in  $u\bar{u}$  and  $d\bar{d}$  events relative to  $s\bar{s}$  events.

Assuming these high-momentum kaons to be directly produced in the fragmentation process, this amounts to a direct observation of a suppression of  $s\bar{s}$  production from the vacuum with respect to  $u\bar{u}$  or  $d\bar{d}$  production. Assuming *all*  $K^\pm$  in the range  $x_p > 0.5$  to be leading, we calculate  $\gamma_s = 0.26 \pm 0.06$ , consistent with values [25] derived from inclusive measurements of the relative production rates of strange and non-strange, pseudoscalar and vector mesons.

Also shown in fig. 10 are the predictions of the three Fragmentation models. All three are consistent with the meson data and with the  $\Lambda^0$  data. The JETSET model is also consistent with the proton data, however the other two models predict a saturated value of  $D_p$  for  $x_p > 0.4$  that is inconsistent with the data.

## 7 Summary and Conclusions

Using the SLD Cherenkov Ring Imaging Detector we have made preliminary measurements of charged pion, kaon and proton production over most of the momentum range in hadronic  $Z^0$  decays. We find the predictions of the JETSET, UCLA and HERWIG fragmentation models to be in qualitative agreement with our data. These results are in agreement with those from previous experiments.

By isolating high-purity light- and  $b$ -flavor samples, we have measured hadron production in light-flavor events, as well as in  $c$ - and  $b$ -flavor events. We find substantial differences in particle production between light- and heavy-flavor events, with the latter producing more mesons overall, but far fewer at high momentum. These qualitative features are expected given the hard fragmentation and high average decay multiplicity of heavy hadrons. The light-flavor sample is more suitable for testing predictions of QCD that assume massless quarks, as well as for testing fragmentation models. We find differences between fragmentation model predictions and our data similar to those found in the inclusive sample, indicating that the deficiencies lie in the simulation of fragmentation rather than in that of heavy hadron production and decay.

By isolating a high-purity gluon jet samples, and comparing with a mixture of light-quark and gluon jets, we have tested the hypothesis that the relative production of charged stable hadrons is the same in light quark and gluon jets. We observe

deviations from equality consistent with those predicted by our simulation to arise from kinematic biases in the jet selection, and conclude that the hypothesis of equality is satisfied to within a few percent.

By isolating high-purity light-quark and light-antiquark samples, we have made the first comparison of hadron and antihadron production in light-quark jets in  $e^+e^-$  annihilation. We observed an excess of  $p$  over  $\bar{p}$ , which appears to increase with momentum, and provides direct evidence for the “leading particle” hypothesis that high momentum protons are more likely to contain the primary quark. We also observed a large excess of high momentum  $K^-$  over  $K^+$  indicating that a high momentum kaon is likely to contain a primary quark or antiquark from the  $Z^0$  decay, and that leading kaons are produced predominantly in  $s\bar{s}$  events rather than  $d\bar{d}$  or  $u\bar{u}$  events. We observe only a small excess of  $\pi^-$  over  $\pi^+$  at high momentum, due in part to the cancellation of the signal from  $u\bar{u}$  and  $d\bar{d}$  events, but also suggesting a large nonleading pion fraction even in this momentum region.

## Acknowledgements

We thank the personnel of the SLAC accelerator department and the technical staffs of our collaborating institutions for their outstanding efforts on our behalf. This work was supported by the U.S. Department of Energy, the UK Particle Physics and Astronomy Research Council (Brunel, Oxford and RAL); the Istituto Nazionale di Fisica Nucleare of Italy (Bologna, Ferrara, Frascati, Pisa, Padova, Perugia); the Japan-US Cooperative Research Project on High Energy Physics (Nagoya, Tohoku); and the Korea Science and Engineering Foundation (Soongsil).

## References

- [1] T.I. Azimov, Y.L. Dokshitzer, V.A. Khoze, S.I. Troyan, *Z. Phys.* **C27** (1985) 65.
- [2] See e.g. I.G. Knowles and G.D. Lafferty, *J. Phys.* **G23** (1997) 731.
- [3] SLD Design Report, SLAC-Report 273, (1984).
- [4] SLD Collaboration: K. Abe *et al.*, *Phys. Rev.* **D51** (1995) 962.
- [5] M.D. Hildreth *et al.*, *Nucl. Inst. Meth.* **A367** (1995) 111.
- [6] C. J. S. Damerell *et al.*, *Nucl. Inst. Meth.* **A400** (1997) 287.
- [7] K. Abe, *et al.*, *Nucl. Inst. Meth.* **A343** (1994) 74.
- [8] SLD Collab., K. Abe *et al.*, *Phys. Rev.* **D59** (1999) 52001.
- [9] S. Brandt *et al.*, *Phys. Lett.* **12** (1964) 57;  
E. Farhi, *Phys. Rev. Lett.* **39** (1977) 1587.

- [10] D. Axen et al., Nucl. Inst. Meth. **A328** (1993) 472.
- [11] D.J. Jackson, Nucl. Inst. Meth. **A388** (1997) 247.
- [12] T. Sjöstrand, Comp. Phys. Comm. **82** (1994) 74.
- [13] P. N. Burrows, Z. Phys. **C41** (1988) 375.  
OPAL Collaboration, M.Z. Akrawy et al., Z. Phys. **C47** (1990) 505.
- [14] SLD Collaboration, K. Abe et al., Phys. Rev. Lett. **79** (1997) 590.
- [15] R. Brun et al., Report No. CERN-DD/EE/84-1 (1989).
- [16] K. Abe, *et al.*, Nucl. Inst. and Meth. **A371** (1996) 195
- [17] DELPHI Collab., P. Abreu *et al.*, Nucl. Phys. **B444** (1995) 3.
- [18] OPAL Collab., P.D. Acton *et al.*, Z. Phys. **C63** (1994) 181.
- [19] ALEPH Collab., D. Buskulic *et al.*, Z. Phys. **C66** (1995) 355.
- [20] S. Chun and C. Buchanan, Phys. Rep. **292** (1998) 239.
- [21] G. Marchesini *et al.*, Comp. Phys. Comm. **67** (1992) 465.
- [22] T.J. Pavel, Ph. D Thesis, Stanford University, January 1997; SLAC-Report-495.
- [23] Particle Data Group, Phys. Rev. **D54** (1996) 1.
- [24] SLD Collab., K. Abe *et al.*, Phys. Rev. Lett. **78** (1997) 3442.
- [25] D.H. Saxon, *High Energy Electron-Positron Physics*, Eds. A. Ali and P. Söding, World Scientific (1988), p. 539.

## \*\*List of Authors

Koya Abe,<sup>(24)</sup> Kenji Abe,<sup>(15)</sup> T. Abe,<sup>(21)</sup> I. Adam,<sup>(21)</sup> H. Akimoto,<sup>(21)</sup> D. Aston,<sup>(21)</sup>  
 K.G. Baird,<sup>(11)</sup> C. Baltay,<sup>(30)</sup> H.R. Band,<sup>(29)</sup> T.L. Barklow,<sup>(21)</sup> J.M. Bauer,<sup>(12)</sup>  
 G. Bellodi,<sup>(17)</sup> R. Berger,<sup>(21)</sup> G. Blaylock,<sup>(11)</sup> J.R. Bogart,<sup>(21)</sup> G.R. Bower,<sup>(21)</sup>  
 J.E. Brau,<sup>(16)</sup> M. Breidenbach,<sup>(21)</sup> W.M. Bugg,<sup>(23)</sup> D. Burke,<sup>(21)</sup> T.H. Burnett,<sup>(28)</sup>  
 P.N. Burrows,<sup>(17)</sup> A. Calcaterra,<sup>(8)</sup> R. Cassell,<sup>(21)</sup> A. Chou,<sup>(21)</sup> H.O. Cohn,<sup>(23)</sup>  
 J.A. Coller,<sup>(4)</sup> M.R. Convery,<sup>(21)</sup> V. Cook,<sup>(28)</sup> R.F. Cowan,<sup>(13)</sup> G. Crawford,<sup>(21)</sup>  
 C.J.S. Damerell,<sup>(19)</sup> M. Daoudi,<sup>(21)</sup> S. Dasu,<sup>(29)</sup> N. de Groot,<sup>(2)</sup> R. de Sangro,<sup>(8)</sup>  
 D.N. Dong,<sup>(13)</sup> M. Doser,<sup>(21)</sup> R. Dubois, I. Erofeeva,<sup>(14)</sup> V. Eschenburg,<sup>(12)</sup>  
 E. Etzion,<sup>(29)</sup> S. Fahey,<sup>(5)</sup> D. Falciari,<sup>(8)</sup> J.P. Fernandez,<sup>(26)</sup> K. Flood,<sup>(11)</sup> R. Frey,<sup>(16)</sup>  
 E.L. Hart,<sup>(23)</sup> K. Hasuko,<sup>(24)</sup> S.S. Hertzbach,<sup>(11)</sup> M.E. Huffer,<sup>(21)</sup> X. Huynh,<sup>(21)</sup>  
 M. Iwasaki,<sup>(16)</sup> D.J. Jackson,<sup>(19)</sup> P. Jacques,<sup>(20)</sup> J.A. Jaros,<sup>(21)</sup> Z.Y. Jiang,<sup>(21)</sup>  
 A.S. Johnson,<sup>(21)</sup> J.R. Johnson,<sup>(29)</sup> R. Kajikawa,<sup>(15)</sup> M. Kalelkar,<sup>(20)</sup> H.J. Kang,<sup>(20)</sup>  
 R.R. Kofler,<sup>(11)</sup> R.S. Kroeger,<sup>(12)</sup> M. Langston,<sup>(16)</sup> D.W.G. Leith,<sup>(21)</sup> V. Lia,<sup>(13)</sup>  
 C. Lin,<sup>(11)</sup> G. Mancinelli,<sup>(20)</sup> S. Manly,<sup>(30)</sup> G. Mantovani,<sup>(18)</sup> T.W. Markiewicz,<sup>(21)</sup>  
 T. Maruyama,<sup>(21)</sup> A.K. McKemey,<sup>(3)</sup> R. Messner,<sup>(21)</sup> K.C. Moffeit,<sup>(21)</sup> T.B. Moore,<sup>(30)</sup>  
 M. Morii,<sup>(21)</sup> D. Muller,<sup>(21)</sup> V. Murzin,<sup>(14)</sup> S. Narita,<sup>(24)</sup> U. Nauenberg,<sup>(5)</sup> H. Neal,<sup>(30)</sup>  
 G. Nesom,<sup>(17)</sup> N. Oishi,<sup>(15)</sup> D. Onoprienko,<sup>(23)</sup> L.S. Osborne,<sup>(13)</sup> R.S. Panvini,<sup>(27)</sup>

C.H. Park,<sup>(22)</sup> I. Peruzzi,<sup>(8)</sup> M. Piccolo,<sup>(8)</sup> L. Piemontese,<sup>(7)</sup> R.J. Plano,<sup>(20)</sup>  
R. Prepost,<sup>(29)</sup> C.Y. Prescott,<sup>(21)</sup> B.N. Ratcliff,<sup>(21)</sup> J. Reidy,<sup>(12)</sup> P.L. Reinertsen,<sup>(26)</sup>  
L.S. Rochester,<sup>(21)</sup> P.C. Rowson,<sup>(21)</sup> J.J. Russell,<sup>(21)</sup> O.H. Saxton,<sup>(21)</sup> T. Schalk,<sup>(26)</sup>  
B.A. Schumm,<sup>(26)</sup> J. Schwiening,<sup>(21)</sup> V.V. Serbo,<sup>(21)</sup> G. Shapiro,<sup>(10)</sup> N.B. Sinev,<sup>(16)</sup>  
J.A. Snyder,<sup>(30)</sup> H. Staengle,<sup>(6)</sup> A. Stahl,<sup>(21)</sup> P. Stamer,<sup>(20)</sup> H. Steiner,<sup>(10)</sup> D. Su,<sup>(21)</sup>  
F. Suekane,<sup>(24)</sup> A. Sugiyama,<sup>(15)</sup> A. Suzuki,<sup>(15)</sup> M. Swartz,<sup>(9)</sup> F.E. Taylor,<sup>(13)</sup>  
J. Thom,<sup>(21)</sup> E. Torrence,<sup>(13)</sup> T. Usher,<sup>(21)</sup> J. Va'vra,<sup>(21)</sup> R. Verdier,<sup>(13)</sup>  
D.L. Wagner,<sup>(5)</sup> A.P. Waite,<sup>(21)</sup> S. Walston,<sup>(16)</sup> A.W. Weidemann,<sup>(23)</sup> E.R. Weiss,<sup>(28)</sup>  
J.S. Whitaker,<sup>(4)</sup> S.H. Williams,<sup>(21)</sup> S. Willocq,<sup>(11)</sup> R.J. Wilson,<sup>(6)</sup>  
W.J. Wisniewski,<sup>(21)</sup> J.L. Wittlin,<sup>(11)</sup> M. Woods,<sup>(21)</sup> T.R. Wright,<sup>(29)</sup>  
R.K. Yamamoto,<sup>(13)</sup> J. Yashima,<sup>(24)</sup> S.J. Yellin,<sup>(25)</sup> C.C. Young,<sup>(21)</sup> H. Yuta.<sup>(1)</sup>

- <sup>(1)</sup> *Aomori University, Aomori, 030 Japan,*  
<sup>(2)</sup> *University of Bristol, Bristol, United Kingdom,*  
<sup>(3)</sup> *Brunel University, Uxbridge, Middlesex, UB8 3PH United Kingdom,*  
<sup>(4)</sup> *Boston University, Boston, Massachusetts 02215,*  
<sup>(5)</sup> *University of Colorado, Boulder, Colorado 80309,*  
<sup>(6)</sup> *Colorado State University, Ft. Collins, Colorado 80523,*  
<sup>(7)</sup> *INFN Sezione di Ferrara and Universita di Ferrara, I-44100 Ferrara, Italy,*  
<sup>(8)</sup> *INFN Laboratori Nazionali di Frascati, I-00044 Frascati, Italy,*  
<sup>(9)</sup> *Johns Hopkins University, Baltimore, Maryland 21218-2686,*  
<sup>(10)</sup> *Lawrence Berkeley Laboratory, University of California, Berkeley, California 94720,*  
<sup>(11)</sup> *University of Massachusetts, Amherst, Massachusetts 01003,*  
<sup>(12)</sup> *University of Mississippi, University, Mississippi 38677,*  
<sup>(13)</sup> *Massachusetts Institute of Technology, Cambridge, Massachusetts 02139,*  
<sup>(14)</sup> *Institute of Nuclear Physics, Moscow State University, 119899 Moscow, Russia,*  
<sup>(15)</sup> *Nagoya University, Chikusa-ku, Nagoya, 464 Japan,*  
<sup>(16)</sup> *University of Oregon, Eugene, Oregon 97403,*  
<sup>(17)</sup> *Oxford University, Oxford, OX1 3RH, United Kingdom,*  
<sup>(18)</sup> *INFN Sezione di Perugia and Universita di Perugia, I-06100 Perugia, Italy,*  
<sup>(19)</sup> *Rutherford Appleton Laboratory, Chilton, Didcot, Oxon OX11 0QX United Kingdom,*  
<sup>(20)</sup> *Rutgers University, Piscataway, New Jersey 08855,*  
<sup>(21)</sup> *Stanford Linear Accelerator Center, Stanford University, Stanford, California 94309,*  
<sup>(22)</sup> *Soongsil University, Seoul, Korea 156-743,*  
<sup>(23)</sup> *University of Tennessee, Knoxville, Tennessee 37996,*  
<sup>(24)</sup> *Tohoku University, Sendai, 980 Japan,*  
<sup>(25)</sup> *University of California at Santa Barbara, Santa Barbara, California 93106,*  
<sup>(26)</sup> *University of California at Santa Cruz, Santa Cruz, California 95064,*  
<sup>(27)</sup> *Vanderbilt University, Nashville, Tennessee 37235,*  
<sup>(28)</sup> *University of Washington, Seattle, Washington 98105,*  
<sup>(29)</sup> *University of Wisconsin, Madison, Wisconsin 53706,*  
<sup>(30)</sup> *Yale University, New Haven, Connecticut 06511.*